ACS APPLIED MATERIALS & INTERFACES

Research Article

www.acsami.org

Fabrication of a Completely Transparent and Highly Flexible ITO Nanoparticle Electrode at Room Temperature

Jungheum Yun,*[,†] Yeon Hyun Park,[‡] Tae-Sung Bae,[§] Sunghun Lee,[‡] and Gun-Hwan Lee[‡]

[†]Advanced Functional Thin Film Department and [‡]Plasma Coating Technology Department, Korea Institute of Materials Science, Changwon, Gyeongnam 641-831, Republic of Korea

[§]Jeonju Center, Korea Basic Science Institute, Jeonju, Jeonbuk 561-180, Republic of Korea

Supporting Information

ABSTRACT: We report the fabrication of a highly flexible indium tin oxide (ITO) electrode that is completely transparent to light in the visible spectrum. The electrode was fabricated via the formation of a novel ITO nanoarray structure, consisting of discrete globular ITO nanoparticles superimposed on an agglomerated ITO layer, on a heat-sensitive polymer substrate. The ITO nanoarray spontaneously assembled on the surface of the polymer substrate by a simple sputter coating at room temperature, without nanolithographic or solution-based assembly processes being required. The ITO nanoarray exhibited a resistivity of approximately 2.3×10^{-3} Ω cm and a specular transmission of about 99% at 550 nm, surpassing all previously reported values of these parameters in the case of transparent porous ITO electrodes synthesized via solution-based processes at elevated temperatures. This novel nanoarray structure and its fabrication methodology can be used for coating large-area transparent electrodes on heat-sensitive polymer substrates, a goal unrealizable through currently available solution-based fabrication methods.

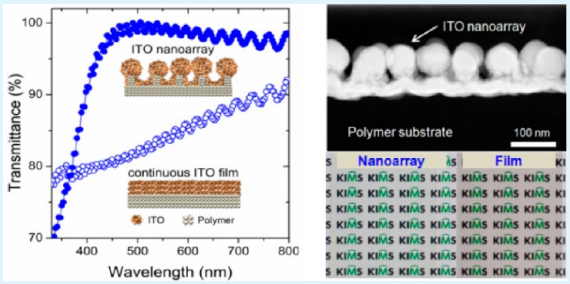

KEYWORDS: *transparent electrode, indium tin oxide, nanoparticles, porous films, flexibility, polymer substrate*

1. INTRODUCTION

Recent advances in technologies for flexible optoelectronic and photonic devices used in liquid crystal displays (LCDs), organic light-emitting diodes (OLEDs), touch screens, thin-film transistors (TFTs), solar cells, e-papers, and sensors have necessitated fabrication of transparent electrodes on highly flexible and heat-sensitive polymer substrates. These applications commonly require electrodes with very specific electrical conductivities and optical transparencies. Conventional film-type electrodes made using tin-doped indium oxide (ITO), a commonly used transparent conductive oxide (TCO), do not meet these requirements owing to serious limitations arising from the inherent material properties of ITO. Apart from its brittleness, the high refractive index of ITO in the visible spectrum range, which is approximately 2.0, causes light incident on an ITO film coated on polymer substrates to be reflected strongly.[1,2] Moreover, its transmission can be optimized only over a narrow bandwidth of visible light. These drawbacks related to the optical properties of ITO cause significant difficulties when the control of the brightness and colors of the images displayed in devices employing film-type ITO electrodes is attempted.

To solve these problems, various alternative transparent electrodes composed of nanostructured materials—including those comprising metal nanopatterns[3] and nanowires,[4−8] carbon nanotubes (CNTs),[7−9] graphenes,[10−12] metal-oxide-based nanowires,[2,13−15] and nanoparticles[16−27]—are emerging as possible alternatives for use in the fabrication of transparent electrodes on polymer substrates. These alternative transparent electrodes show structural durability even when the underlying flexible polymer substrates are subjected to deformation-causing stresses. However, their performances are constrained by the trade-off between their optical transparency and electrical conductivity values. This is because improvements in the conductivity of the electrodes usually require an increase in their thickness or density, and this seriously affects their optical transparency.[1,3] As a result, the transparency achievable in these alternative electrodes does not surpass that of ITO films in the visible spectrum range.[1] Electrodes fully transparent to light in the visible spectrum range have not yet been fabricated because their fabrication calls for the independent control of their optical transparency in a manner that does not deteriorate their conductivity.

Among the alternative electrodes being investigated, ITO-nanoparticle-based porous coatings have received significant attention because these porous ITO coatings have a comparative advantage over other alternatives when it comes to the optical transparency. The optical transparency of the porous ITO coatings is not affected significantly by an increase in the thickness or density of the coatings. These porous ITO

Received: October 15, 2012
Accepted: December 5, 2012
Published: December 5, 2012

coatings are predominantly fabricated by solution-based processes that have the potential to enable the fabrication of the coatings on large-area polymer substrates. However, the process temperature is a key obstacle to using the solution-based processes with heat-sensitive polymer substrates. Although the individual ITO nanoparticles used in the solution-based processes exhibit low resistivity (approximately 10^{-4} Ω cm), the highly porous structure of the coatings, which is designed for improving the optical transparency, usually requires the formation of interconnections between the nanoparticles at elevated sintering temperatures so that the resistivity increases and is in the range of 10^{-1} to 10^{-2} Ω cm.[20] The reported resistivity values are usually greater than 1×10^{-2} Ω cm even when the sintering temperatures are higher than 300 °C. In addition, the optical transmission is as high as 90%.[16,21] Recently, Lee et al. reported the fabrication of coatings whose electrical conductivity and optical transparency values surpassed the previously reported highest values in the case of porous ITO coatings synthesized via solution-based coating processes.[22] A resistivity of 5×10^{-3} Ω cm, corresponding to a sheet resistance of 356 Ω sq^{-1}, and a transmission of 93% were achieved in an porous ITO coating that was sintered at 300 °C. On the other hand, as the result of efforts to lower the sintering temperature required, porous ITO coatings with a resistivity in the range of 10^{-1} Ω cm (a sheet resistance of >400 Ω sq^{-1}) and an optical transparency of 85−90% have also been fabricated at a relatively low sintering temperature of about 130 °C by employing various sintering strategies.[23−27] However, in spite of the aforementioned efforts, further improvements in the electrical conductivity and the optical transparency and a further lowering of the sintering temperature are still required for the fabrication of field-applicable porous ITO coatings as transparent electrodes on heat-sensitive polymer substrates.

In this study, a porous ITO electrode with a novel nanoarray structure was fabricated on flexible heat-sensitive polyethylene terephthalate (PET) substrates by a simple vacuum coating process at room temperature without requiring a post-deposition high-temperature sintering process. This electrode, which exhibited a minimum resistivity of 2.3×10^{-3} Ω cm (a sheet resistance of 230 Ω sq^{-1}), could suppress the reflection of light and was almost completely transparent over the entire visible light spectrum. The electrode nanoarray exhibited a unique hybrid structure that consisted of a periodic arrangement of discrete, globular ITO nanoparticles superimposed on an agglomerated ITO layer. The dimensions and periodicity of the nanoarray could be controlled precisely to within tens of nanometers in order to tune its refractive index, and thus, minimize the reflection of incident light. More importantly, the nanoarray assembled spontaneously on the polymer surface owing to a unique plasma-based treatment of the polymer surface prior to the ITO deposition.

2. EXPERIMENTAL METHODS

2.1. Materials. The substrates used in this study were highly flexible and transparent and were made of PET. They had a thickness of 125 μm, and they were purchased from Panac Co. The surface of the untreated PET substrate was very smooth, and its root-mean-square (RMS) surface roughness was about 1 nm, as evaluated using the tapping mode of an atomic force microscope (AFM) (Digital Instruments, NanoScope-IIIa) and commercially available Si cantilevers tips (Veeco). It is noteworthy that very similar results were obtained for PET substrates purchased from different suppliers. In_2O_3 with 3 wt % Sn was used as the target material for the sputtering of ITO and was procured from Advanced Nano Products Co. Ltd.

2.2. Fabrication of ITO Nanoarrays. The plasma pretreatment of the polymer substrates was performed in a home-built glow-discharge plasma system using a 13.56 MHz capacitively coupled plasma (CCP) supply. The system consisted of a plate electrode with a diameter of 6 in. and a gas showerhead with a diameter of 6 in. made from a ring-shaped stainless steel tube with a diameter of 0.23 in. The showerhead was at a distance of 15 cm from the electrode. The showerhead and chamber wall were grounded during the polymer pretreatment process. After the polymer substrates were placed on the plate electrode, the chamber was evacuated and the pressure reduced to a vacuum level of 6.7 Pa. Then, the pressure was increased to 22.7 Pa because of the flow of Ar gas (99.999%) into the chamber through the showerhead at a flow rate of 50 sccm. The plasma pretreatment of the PET surface was carried out for different periods, ranging from 1 to 7 min, at a radio frequency (RF) power of 1.1 W cm^{-1}. To analyze the plasma parameters for the pretreatment of the PET surface, the electron temperature and ion fluence were derived from the $I-V$ characteristics that were determined using a double-probe system. Further, the ion energy was determined from the self-bias and was found to be identical to the plasma potential in the system. The energy and fluence rate of the ions that impinged upon the surfaces of the polymer substrates were measured to be 102 eV and 3.1×10^{17} cm^2, respectively, for pretreatment for 1 min duration. During the pretreatment process, the temperature of the PET surface was kept below 50 °C, which was sufficiently lower than the glass transition temperature of PET of around 80 °C.

The sputtering-based deposition of the ITO nanoarrays was subsequently performed on the plasma-treated PET surfaces using a separate home-built radio frequency (RF) (13.56 MHz) magnetron sputtering system with ITO targets with a length of 39.5 cm and a width of 9.5 cm. The chamber was initially evacuated to 6.7×10^{-4} Pa prior to the sputtering, and the chamber pressure was then increased to 0.31 Pa by introducing Ar gas (99.9999%) at a flow rate of 22 sccm. An RF power of 200 W (0.53 W cm^{-2}) was used to initiate the sputtering process. The size of ITO nanoparticles in the ITO nanoarray was varied from 30 nm to 100 nm by changing the deposition time. In addition, the temperatures of the PET surfaces were kept below 50 °C during the sputtering process.

2.3. Characterization. The morphologies of the surfaces of the PET substrates after the plasma-based pretreatment and the subsequent deposition of the ITO nanoarrays were determined using an ultra-high-resolution (UHR) field-emission scanning electron microscope (FE-SEM) (Hitachi, S-5500). An electron beam at a low accelerating voltage of 2 kV was used in order to prevent PET surfaces from being seriously damaged by the radiation during the imaging process. The cross-sectional structure and corresponding composition of the ITO nanoarrays were determined by scanning transmission electron microscopy (STEM) (FEI, Titan) and energy-dispersive X-ray spectroscopy (EDS). The specimens were cross-sectioned on a cryo-stage (Gatan, Alto 2500), kept at −154 °C, using a dual-beam-focused ion beam system (FEI, Quanta 3D) in order to minimize thermal damage during the ion-beam milling. For the STEM measurements, the specimens were placed on a cryo-stage and were analyzed at a voltage of 80 kV.

The specular transmission and reflection spectra of the ITO nanoarrays were measured at normal incidence for radiation with wavelengths between 320 and 800 nm using an ultraviolet-visible (UV-Vis) spectrophotometer (Cary 5000, Varian). The refractive index and porosity of the ITO nanoarrays were determined using a spectroscopic ellipsometer (Ellipso Technology, Elli-SEU-am12). The spectroscopic ellipsometry measurement was carried out at the angle of incidence of 70° over the energy range between 1.2 and 5.2 eV. The refractive index and absorption coefficient were determined by using the Lorentz oscillator dispersion model. Two or three different layers, each having different refractive index values, were analyzed for an ITO nanoarray because the spacing between neighboring ITO nanoparticles changed along the normal direction owing to the globular geometry of the

nanoparticles. As a result, the refractive index varied widely even within a single ITO nanoarray.

The sheet resistance of ITO nanoarrays was determined as the average value of at least three different 3 cm × 3 cm samples, for each growth conditions by using a four-point probe system (MCP-T600, Mitsubishi chemical Co.). The resistivity was then calculated from the sheet resistance and the thickness of the entire nanoarray. The electrical conductivity of the nanoarrays under stress was measured through two-point bending techniques, including the irreversible bending test and the cyclic bending test. ITO nanoarrays were deposited on PET substrates with a length of 5 cm and a width of 1.5 cm, and these substrates were used as the test specimens for the bending tests. With respect to the irreversible bending test, the change in the electrical resistance of the ITO nanoarrays was measured as a function of the bending radius, which was approximately half the distance between the two plates of the bending system. With respect to the cyclic bending test, the change in the electrical resistance was measured as a function of the bending cycles. In the irreversible bending test, the movable plate was made to approach the fixed plate at a rate of 0.2 mm s^{-1} until a change in the resistance of the ITO nanoarrays corresponding to electrical failure was detected. In the cyclic bending test, the change in resistance was evaluated using a displacement rate of 10 mm s^{-1}. During the cyclic bending test, the test specimens were subjected to multiple bending cycles (2700 cycles in this case) with the minimum bending radius being 5 mm. The thicknesses of the continuous ITO films formed on Si wafers were determined using a surface profilometer (P-11, KLA-Tencor), whereas the size of the ITO nanoparticles was determined from the cross-sectional FE-SEM and STEM images of the specimens. The temperatures of the PET surfaces during the polymer pretreatments and the ITO sputtering processes were measured using thermal labels (Nichiyu Giken Kogyo).

3. RESULTS AND DISCUSSION

3.1. Fabrication of ITO Nanoarrays on Polymer Substrates. ITO nanoarrays were synthesized on PET substrates by using a simple vacuum deposition technique comprising the following two steps: (i) the pretreatment of the surface of the PET substrate with Ar plasma and (ii) the subsequent magnetron sputter coating of the ITO nanoarray (Figure 1). After the plasma-based pretreatment of the PET substrate, nanoscopic protrusions with typical dimensions in the range of tens of nanometers formed on the surface of the polymer substrate. The existence of these polymeric protrusions was an indispensable requisite for the formation of the ITO nanoarray on the surface of the PET substrate. The deposition of an ITO coating on a pristine PET surface that did not have these protrusions simply led to the formation of a uniform layer of ITO on the substrate (Figure 1a). This film-like ITO layer was similar to those of ordinary oxides deposited on polymers using conventional vacuum-coating processes. The average size and periodicity of the nanoscopic polymeric protrusions were strongly affected by the duration of the plasma-based pretreatment of the PET substrate (Figure 1b, c). Debate on the exact mechanism responsible for the formation of these polymeric protrusions continues. However, the most likely explanation is that they developed on the topmost surface of the PET substrate during the pretreatment because small molecular chains of the polymer generated by polymer-chain scission and etching reaccumulated on the surface of the PET substrate. They then agglomerated in order to reduce the difference in the free energy of the modified top surface and that of the underlying, untouched bulk of the polymer substrate.[28−32]

The polymeric protrusions abruptly transformed the morphology of the substrates from a two- to a three-

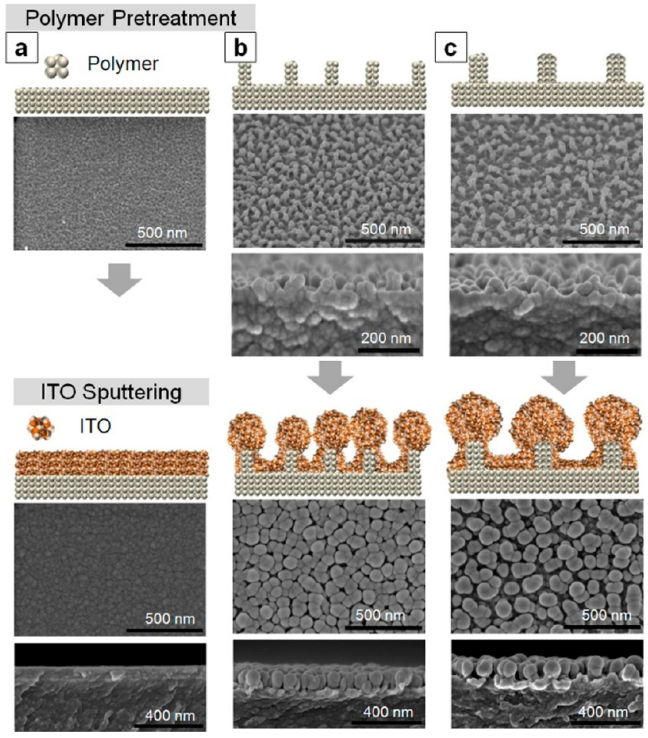

Figure 1. Schematic diagrams and corresponding FE-SEM images demonstrating the evolution of the ITO nanoarrays on the surfaces of polymer substrates that were pretreated under various conditions: (a) a continuous ITO layer on a pristine, untreated polymer surface, (b) a compact ITO nanoarray on a polymer surface that was pretreated for a relatively short period of 1 min, and (c) a loose ITO nanoarray on a polymer surface that was pretreated for an extended period of 3 min.

dimensional one for the subsequently deposited ITO coating. It was observed that the ITO coating did not completely wet the surface of the PET substrate owing to the presence of the polymeric protrusions. FE-SEM images (Figure 1b, c) showed that the ITO coating formed globular nanoparticles on the polymeric protrusions. The structure and composition of the ITO nanoarray were further evaluated using cross-sectional STEM images (Figure 2) and EDS (see Figure S1 in the Supporting Information). It was found that the nanoarray of ITO, which had 3 wt % Sn, consisted of discrete globular ITO nanoparticles with an average size of 70 nm superimposed on an agglomerated ITO layer with an average thickness of 30 nm. The sputtering process at room temperature produced an amorphous ITO nanoarray that was verified by its diffraction pattern. The self-sustaining growth of the ITO nanoarray on the polymeric protrusions was clearly distinguishable from the growth of continuous ITO layers on pristine polymer surfaces.

The selective self-assembly of the ITO nanoparticles on the polymeric protrusions provided an opportunity for manipulating the periodicity of the ITO nanoparticles by changing the parameters of the polymer pretreatment. Increasing the pretreatment time changed the number density of the polymeric protrusions and therefore the average distance between neighboring protrusions. When the duration of the pretreatment was increased from 1 min (Figure 1b) to 3 min (Figure 1c), the average distance between neighboring protrusions increased from roughly 70 to 110 nm as a result of the decrease in the number density of the protrusions. Furthermore, the number density and average interparticle distance of the subsequently grown ITO nanoparticles was

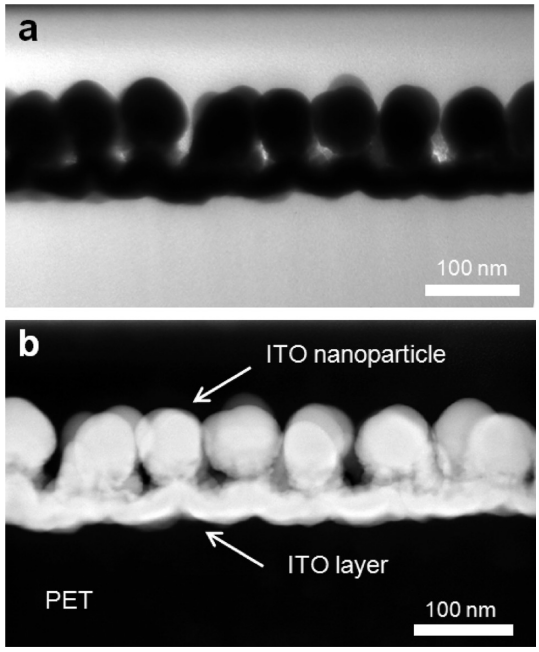

Figure 2. (a) TEM bright-field image and (b) high-angle annular-dark-field image of an ITO nanoarray coated on a PET surface that was pretreated with Ar plasma for 3 min.

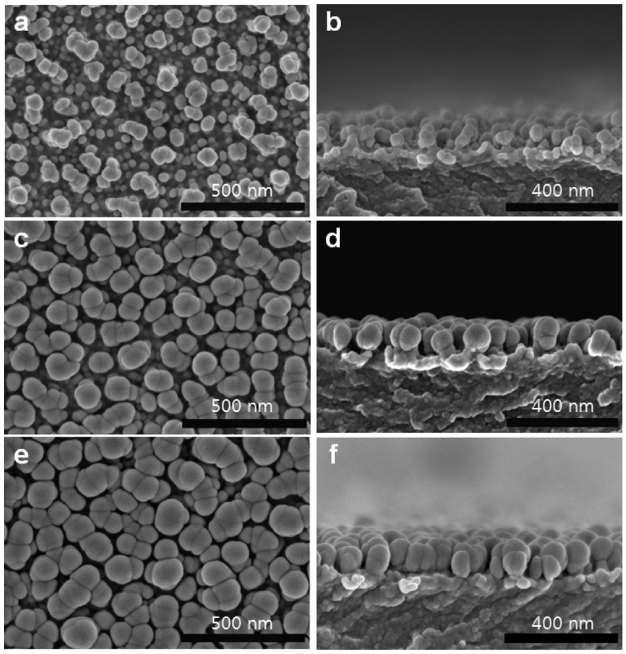

Figure 3. Evolution of the ITO nanoparticles on the polymeric protrusions. (a, c, and e) Plane and (b, d, and f) cross-sectional FE-SEM images of the ITO nanoarrays of nanoparticles of different sizes: (a and b) 30 nm, (c and d) 70 nm, and (e and f) 90 nm.

dictated by the corresponding values of these parameters for the polymeric protrusions. An increase in the average distance between neighboring ITO nanoparticles was clearly observed in the case of a PET surface pretreated for 3 min (Figure 1c), whereas the ITO nanoparticles on a PET surface pretreated for only 1 min tended to coalesce with one another, resulting in the distances between neighboring nanoparticles being very small (Figure 1b).

During the early stages of the deposition process, ITO nanoparticles were seen to grow over most of the PET substrate, regardless of whether the ITO nanoparticles were formed on the polymeric protrusions or on the recessed surfaces between protrusions (Figure 3). As the deposition process progressed, ITO nanoparticles continued to grow on the protrusions owing to a ready supply of reactive species with relatively large fluxes. On the other hand, the growth of ITO nanoparticles on the spaces between the protrusions was not as steady. The growth of the nanoparticles on the recessed surfaces was hindered because of a shortage of the reactive species. This was due to a shadowing effect caused by the fast growth of the ITO nanoparticles on the polymeric protrusions. As a result, the nanoparticles formed on the polymeric protrusions grew large while those formed on the recessed surfaces between the protrusions did not. However, a continuous ITO layer was formed by the coalescence of the smaller ITO nanoparticles as they were densely distributed on the recessed surfaces. The other morphological peculiarity of the ITO nanoarray, i.e., the globular shape of the discrete ITO nanoparticles formed on the polymeric protrusions, can be attributed to the fact that the lateral expansion of the ITO nanoparticles along the top surface of the protrusions, which had sharp and irregular curvatures, was restricted by poor polymer-to-oxide adhesion, which was much weaker than the cohesion between the oxide molecules of the nanoparticles.[33] The ITO nanoparticles were in contact with only the top parts of the protrusions, and there was no increase in the area of contact between the nanoparticles and the protrusions. Thus, the ITO nanoparticles exhibited a spherical geometry, which led to the energy of their surfaces being minimized. Furthermore, these morphological characteristics of the ITO nanoarray were not affected appreciably by any change in the free energy of the pretreated PET surface owing to the exposure of the PET surface to the ambient atmosphere before the ITO deposition. If the formation of globular ITO nanoparticles is compatible with the sputtering of other TCO materials on polymer substrates that show nanosized polymeric protrusions, this method can be applied universally for the direct formation of nanoparticles of various conductive oxide materials on polymer substrates while being able to control precisely the doping levels.

3.2. Optical Properties of the ITO Nanoarray. The formation of ITO nanoparticles with average interparticle distances and sizes within the sub-100 nm scale, which were well below the wavelengths of light in the visible spectrum and thus prevented the interference of the incident light, afforded surfaces with highly antireflective (AR) characteristics in the visible spectrum range by the tuning of the refractive index of the ITO nanoarray. The refractive index required for optimal AR characteristics was predicted using a square root approximation of the refractive index of PET, which was about 1.65, and was found to be approximately 1.3. This low value of the refractive index of the ITO nanoarray was successfully achieved by increasing the average distance between neighboring ITO nanoparticles, which directly corresponded to an increase in the porosity of the ITO nanoarray (Figure 4). The continuously varied spacing between neighboring ITO nanoparticles caused a nonnegligible fluctuation in the refractive index ranging between 0.1 and 0.2 at a wavelength for a single ITO nanoarray. Therefore, the refractive index of an ITO nanoarray was represented as the range between its maximum and minimum values instead of

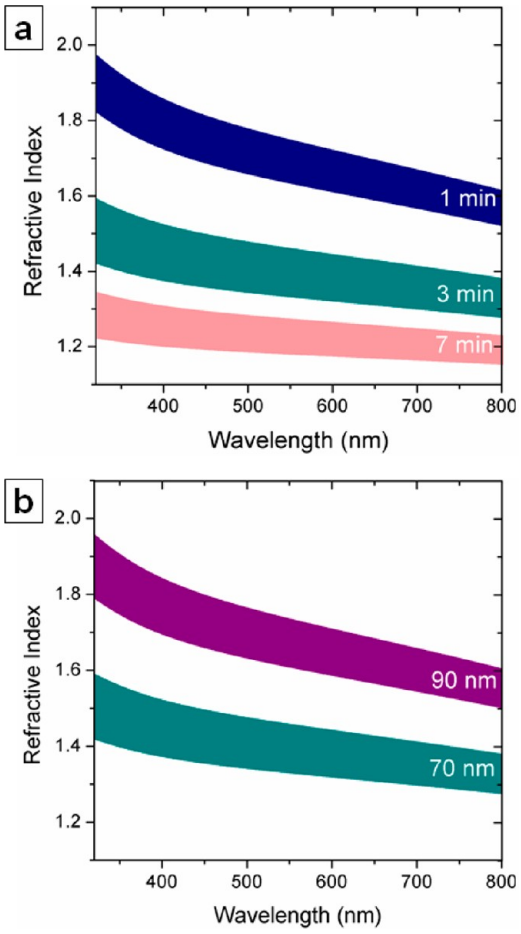

Figure 4. Refractive indices, measured by ellipsometry, of the various ITO nanoarrays in the visible spectrum. The wavelength dependence of the refractive index was determined for (a) different pretreatment periods, 1, 3, and 7 min, with the size of the nanoparticles being constant at 70 nm and (b) different nanoparticle sizes, 70 and 90 nm, with the pretreatment period being constant at 3 min.

single value. The ellipsometry results showed that the value of the refractive index steadily decreased with an increase in the pretreatment duration from 1 to 7 min (Figure 4a). The refractive index decreased to approximately 1.4−1.5 for a pretreatment of 3 min and to 1.2−1.3 for a pretreatment of 7 min, at a wavelength of 550 nm. However, an increase in the size of the ITO nanoparticles to values greater than 70 nm led to a deterioration of the AR characteristics because of an increase in the refractive index (Figure 4b).

The decrease in the refractive index resulted in the ITO nanoarray being transparent in the visible spectrum range. The AR characteristics of the ITO nanoarray were optimal when the pretreatment was 3 min in duration and the size of the nanoparticles was 70 nm (Figure 5). The optimized ITO nanoarray was confirmed to be transparent at wavelengths greater than 430 nm as the reflection of the incident light was suppressed effectively. Specular reflection in the case of a PET substrate coated with the optimized ITO nanoarray was even lower than that in the case of an uncoated PET substrate (see Figure S2 in the Supporting Information). The AR characteristics of the optimized ITO nanoarray contributed directly to the increase in the specular transmission. The specular transmission of the optimized ITO nanoarray was compared with that of a 70-nm-thick continuous ITO film deposited on a pristine PET surface that did not have the polymeric protrusions. It was found that the specular transmission of the former was higher (99%) than that of the latter (82%) at a wavelength of 550 nm (Figure 5a). This difference in the transmissions of the ITO nanoarray and the continuous film can be seen clearly in the photograph shown in Figure 5c. The optimized ITO nanoarray was used to successfully fabricate a highly flexible, transparent electrode on a large-area PET substrate with a size of 12 × 12 cm^2 (Figure 5d).

The AR characteristics of the ITO nanoarray were very sensitive to changes in the duration of the pretreatment. The transmission of the array decreased sharply when the duration of the pretreatment deviated from 3 min (Figure 5b). For a pretreatment duration of 1 min, the ITO nanoarray exhibited a noticeable increase in its reflection because of the sharp increase in its refractive index, as can be seen from Figure 4a. On the other hand, although a longer pretreatment resulted in a lower refractive index over the visible spectrum range, an increase in the pretreatment duration from 3 to 7 min actually caused an increase in the reflection for shorter wavelengths in the visible spectrum. This was because the average distance between neighboring ITO nanoparticles approached the threshold level, at which the incident light with short wavelengths would experience interference in the ITO nanoarray (see Figure S2 in the Supporting Information). The deterioration of the AR characteristics owing to the interference undergone by the incident light led to a sharp decrease in the transmission of the nanoarray at the related wavelengths. A similar result was obtained when the size of the ITO nanoparticles was increased to values greater than 70 nm (Figure 5a). It is worth noting that this large degree of deterioration in the AR characteristics occurred with even slight variations—within the range of tens of nanometers—in the average interparticle distance and size of the nanoparticles.

3.3. Electrical and Structural Properties of the ITO Nanoarray. The sheet resistance of the ITO nanoarray reached its minimum value at the conditions for which the AR characteristics were optimal, i.e., as a pretreatment duration of 3 min and a nanoparticles size of 70 nm (Figure 6). The sheet resistance did not decrease beyond 230 Ω sq^{-1}, which corresponded to a resistivity of 2.3 × 10^{-3} Ω cm (this was calculated using the thickness of the entire nanoarray), with increases either in the size of the ITO nanoparticles to values greater than 70 nm (Figure 6a) or in the pretreatment time to values greater than 3 min (Figure 6b). These results indicated that the agglomerated ITO layer that was deposited between the polymer surface and the ITO nanoparticles played a vital role in determining the electrical conductivity of the ITO nanoarray. In other words, the agglomerated ITO layer provided the predominant conductive path in the ITO nanoarray, whereas the discrete globular ITO nanoparticles superimposed on the agglomerated ITO layer did not contribute substantially to the electrical conductivity of the overall ITO nanoarray. As a result, the increase in the thickness of the agglomerated ITO layer led to the decrease in the sheet resistance of the ITO nanoarray. An increase in the overall dimensions of the ITO nanoarray corresponded directly to an increase in the thickness of this agglomerated ITO layer until the growth of the agglomerated ITO layer was hindered by the shadowing effect due to ITO nanoparticles that formed on the polymeric protrusions. The growth of the agglomerated ITO layer was terminated with its maximum thickness of about 30 nm as the size of the ITO nanoparticles reached 70 nm at a

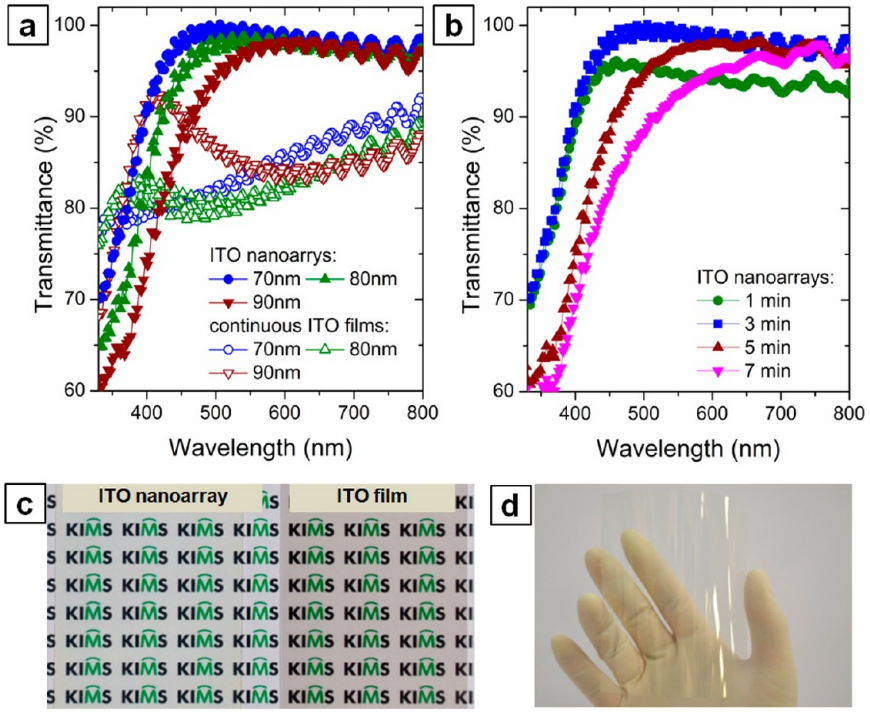

Figure 5. (a) Dependence of the specular transmission of the ITO nanoarrays on the size of the ITO nanoparticles. The transmission of the ITO nanoarrays was compared with that of continuous ITO films. The ITO nanoarrays were developed on PET surfaces that were pretreated for 3 min whereas the continuous ITO films were developed on untreated PET surfaces. The transmission of ITO nanoarrays was measured by excluding that of the PET substrate. (b) Dependence of the transmission of the ITO nanoarrays having 70-nm-sized nanoparticles on the polymer pretreatment period. (c) Comparison of the ITO nanoarray with 70-nm-sized nanoparticles and a continuous ITO film with a thickness of 70 nm. (d) A photograph of a highly flexible, transparent PET substrate coated with ITO nanoarrays having 70-nm-sized nanoparticles fabricated after pretreating the PET substrate for a period of 3 min.

pretreatment time of 3 min. A further growth of the ITO nanoarray corresponding to the increase in the size of the ITO nanoparticles was not accompanied by a decrease in the sheet resistance, and thus, it had a negative effect on the electrical conductivity of the overall ITO nanoarray by increasing the resistivity. The decrease in the sheet resistance with an increase in the pretreatment time to up to 3 min was closely associated with the increase in the average distance between neighboring ITO nanoparticles. A greater average distance led to the development of a thicker ITO layer on the recessed surfaces as the occurrence of the shadowing effect was in effect delayed. However, the effect was saturated when the duration of the pretreatment was greater than 3 min.

The performance of the ITO nanoarray as a transparent electrode was compared with that of continuous ITO films that were coated on pristine PET substrates, with the sputtering conditions being the same as those used to form the ITO nanoarray in this study. The performance was also compared to those previously reported for porous ITO films fabricated via solution-based processes at elevated sintering temperatures (Figure 7a).[21,22,24,25,27] The sheet resistance of the ITO nanoarray was close to the lowest value reported for porous ITO films formed via solution-based processes. In addition, the transmission of the ITO nanoarray was about 6% higher than the highest value reported for the porous ITO films. The transmission of the ITO nanoarray was at least 12% higher than that of the continuous ITO films. Even though the sheet resistance of the ITO nanoarray was about 3−4 times higher than that of the continuous ITO films, it was low enough to allow the nanoarray to be used for several applications, including in resistive touch panels.

The performance of the transparent electrode was further evaluated by comparing a figure of merit (FoM) of the ITO nanoarray and that of the continuous ITO film (Figure 7b). This FoM was reflective of the transmission and the sheet resistance of the two entities and was given by the following expression: FoM = T^{10}/R_s, where T is the specular transmission and R_s is the sheet resistance of the entities.[34] The value of the FoM of the ITO nanoarray remained over $3 \times 10^{-3}\ \Omega^{-1}$ for the entire range of nanoparticle sizes examined, with a higher value of the FoM suggesting a better performance of the corresponding entity as a transparent electrode. The ITO nanoarray outperformed the continuous ITO continuous film for thicknesses lower than or equal to 80 nm. The value of the FoM for the continuous ITO film was higher than that of the ITO nanoarray for thicknesses greater than 80 nm. This was because of the saturation in the sheet resistance of the nanoarray at the higher thickness values. Thus, the ITO nanoarray can be a more suitable choice than the continuous ITO film when a thin electrode is required such that it maintains its structural durability on highly flexible polymer substrates.

The structural durability of the ITO nanoarray was tested by exposing it to high tensile stresses, which were induced by bending the PET substrate (Figure 8). When bent, cracks propagated across the entire width of the specimen and were considered to be the main cause of the structural failure and the consequent electrical failure of the ITO nanoarray.[35−37] The electrical failure of the ITO nanoarray was determined by measuring the change in the electrical resistance of the ITO nanoarray while the PET substrate was subjected to tensile stresses by bending (Figure 8a). The relative increase in its

dx.doi.org/10.1021/am302341p | ACS Appl. Mater. Interfaces 2013, 5, 164−172

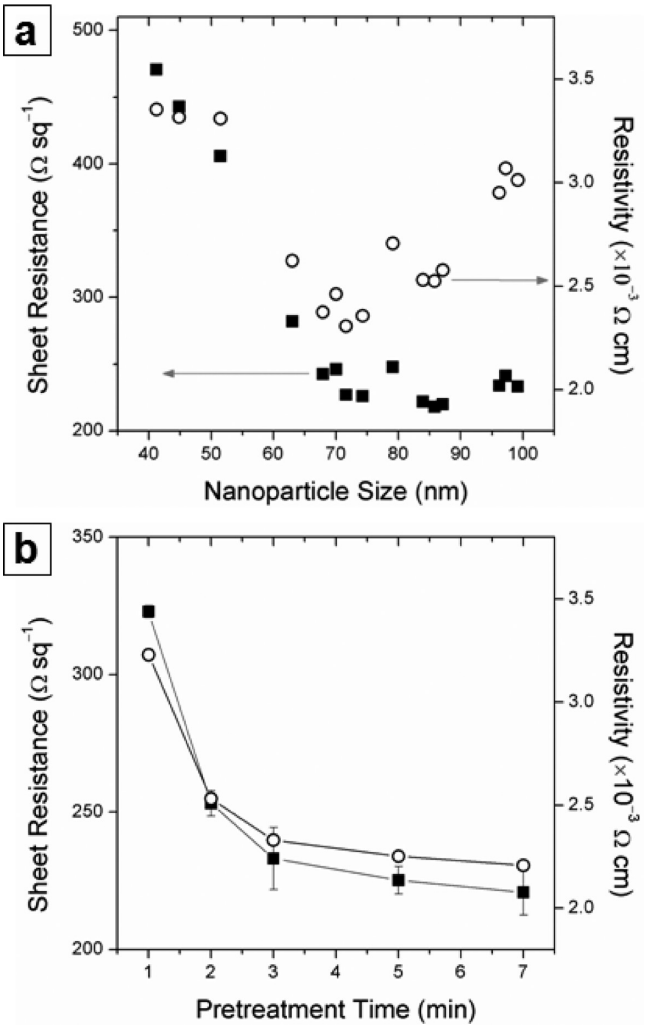

Figure 6. Dependence of the resistivity and sheet resistance of the ITO nanoarrays on (a) the nanoparticle size, with the pretreatment period being constant at 3 min and (b) the duration of pretreatment of PET surfaces, with the size of the nanoparticles being constant at 70 nm.

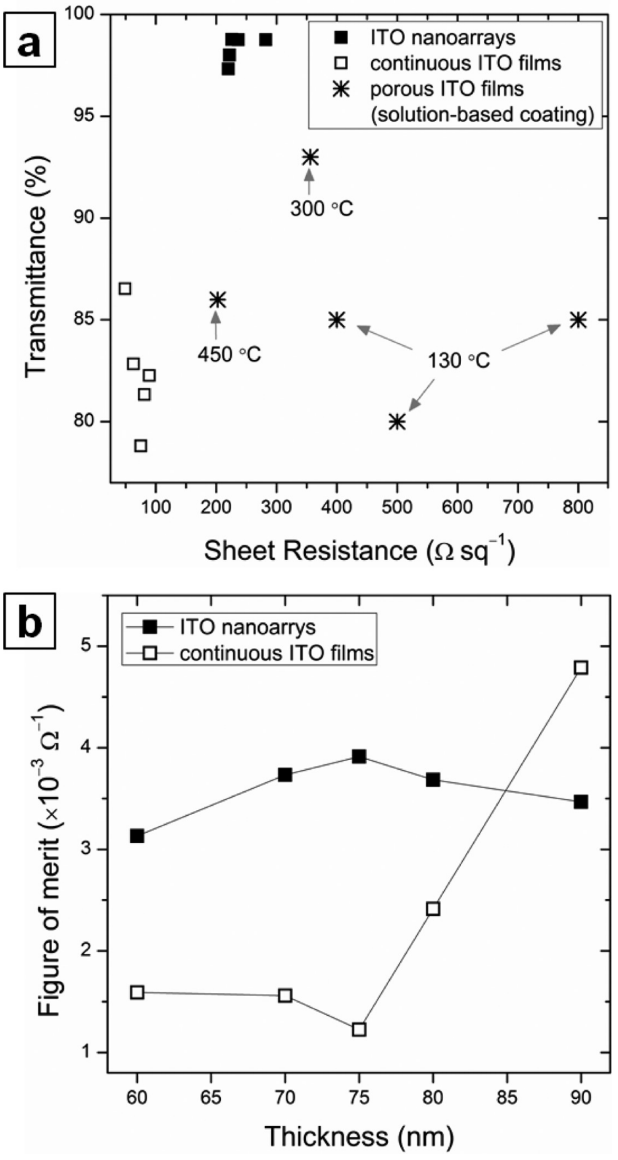

Figure 7. (a) Comparison of the specular transmissions of various transparent electrodes plotted as functions of their sheet resistances. The transmissions of the ITO nanoarrays and continuous ITO films were compared with that of porous ITO films that were coated via solution-based processes at the following sintering temperatures: 130,[25,26,28] 300,[23] and 450 °C.[22] The transmissions were measured at a wavelength of 550 nm. (b) Comparison of the figure of merit of the ITO nanoarrays and continuous ITO films. The ITO nanoarrays were coated on PET surfaces that were pretreated for 3 min.

resistance was measured using the following expression, $(R - R_0)/R_0$, where R_0 is the initial resistance and R is the resistance under tensile stress. For the irreversible two-point bending test, the test specimen comprised an optimized ITO nanoarray made up of 70-nm-sized nanoparticles superimposed on a 30-nm-thick ITO layer. The specimen did not fail until the bending radius was reduced to less than 4 mm (Figure 8b). On the other hand, a test specimen comprising a continuous ITO film having a thickness of 70 nm failed at a bending radius of 7 mm. The absolute sheet resistance of the continuous ITO film became greater than that of the ITO nanoarray at the bending radius of 7 mm (see Figure S3a in the Supporting Information). The failures of both the ITO nanoarray and the continuous film can be ascribed to the abrupt propagation of microscopic cracks in a direction perpendicular to that of the tensile load.[37] Since the tensile strain induced by the bending is directly proportional to the bending radius,[38] it is expected that the tensile strain leading to the failure of the ITO nanoarray is about 1.8 times larger than the strain leading to the failure of the continuous ITO film. The structural durability of the ITO nanoarray on a highly deformed polymer substrate was further evaluated by performing cyclic bending tests (Figure 8c and Figure S3b in the Supporting Information). The ITO nanoarray could withstand 2700 bending cycles at a minimum bending radius of 5 mm, and it did not show any change in its resistance. On the other hand, the continuous ITO layer failed completely after a single bending cycle at the same bending radius. The results of the bending tests support the conclusion that the geometry of the ITO nanoarray lessened the build-up of stress and thus improved its structural and electrical durabilities against externally induced stresses.

4. CONCLUSION

We were able to fabricate an ITO electrode that was completely transparent to light in the visible spectrum. This was done by

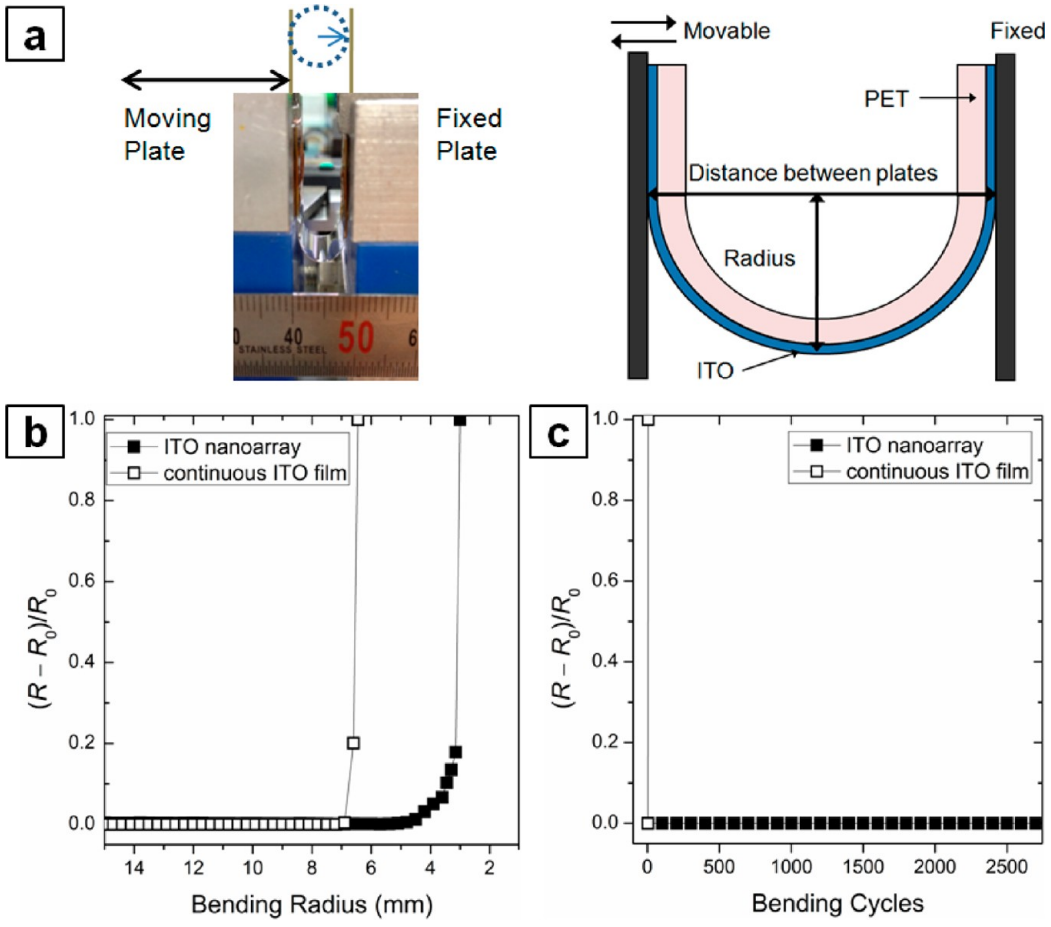

Figure 8. (a) Photograph and corresponding schematic diagram of the two-point bending test system. The normalized resistance changed (b) as a function of the bending radius during the irreversible bending test and (c) as a function of the bending cycle, with the bending radius being constant at 5 mm.

the synthesis of a novel structure in the form of an ITO nanoarray, consisting of discrete globular nanoparticles superimposed on an agglomerated ITO layer with sub-100 nm dimensions, on a PET substrate. A simple vacuum deposition process consisting of plasma-based polymer pretreatment and subsequent sputter deposition of ITO was successfully used to form the nanoarray directly on the surface of the PET substrate at room temperature. A nearly periodic pattern of discrete ITO nanoparticles could be developed on the polymer substrates, without complicated lithographic nanopatterning or solution-based nanoparticle fabrication techniques. Complete transparency was achieved at a minimum sheet resistance and resistivity of approximately 230 Ω sq^{-1} and 2.3 × 10^{-3} Ω cm, respectively, by controlling the size of and the average distance between the nanoparticles within a range of tens of nanometers. The complete transparency and excellent flexibility of the nanoarray will afford a large degree of freedom in the fabrication of transparent electrodes on highly flexible polymers. In addition, the synthesis method can be readily adapted to fabricate transparent electrodes using other oxide materials on large polymer substrates at high throughputs.

■ ASSOCIATED CONTENT

Supporting Information

A cross-sectional TEM image and the corresponding EDS spectra of the ITO nanoarrays coated on the surface of a PET substrate. Specular reflectance spectra of the ITO nanoarrays with different sized nanoparticles and pretreatment times. Changes in the absolute sheet resistances of the ITO nanoarrays and the continuous ITO films as functions of the bending radius and the bending cycle. This material is available free of charge via the Internet at http://pubs.acs.org/.

■ AUTHOR INFORMATION

Corresponding Author

*Address: 797 Changwondaero, Changwon, Gyeongnam, 641−831, Republic of Korea. E-mail: jungheum@kims.re.kr. Tel: +82 (0)552803515. Fax: +82 (0)552803570.

Notes

The authors declare no competing financial interest.

■ ACKNOWLEDGMENTS

This research was funded by the World Premier Materials (WPM) program and by an internal grant from the Korea Institute of Materials Research. The authors thank Dr. G. Kim, Mr. N. Hong and Mr. C. Kwon of the Korean Institute of Science and Technology (KIST) for their help with the TEM measurements. The ellipsometric measurements to determine the refractive indices were performed at Ellipso Technology Co., Ltd.

■ REFERENCES

(1) Hecht, D. S.; Hu, L.; Lrvin, G. *Adv. Mater.* **2011**, *23*, 1482−1513.

(2) Wu, H.; Hu, L.; Carney, T.; Ruan, Z.; Kong, D.; Yu, Z.; Yao, Y.; Cha, J. J.; Zhu, J.; Fan, S.; Cui, Y. *J. Am. Chem. Soc.* **2011**, *133*, 27−29.
(3) Kuang, P.; Park, J.-M; Leung, W.; Mahadevapuram, R. C.; Nalwa, K. S.; Kim, T.-G.; Chaudhary, S.; Ho, K.-M.; Constant, K. *Adv. Mater.* **2011**, *23*, 2469−2473.
(4) Lee, J.-Y.; Connor, S. T.; Cui, Y.; Peumans, P. *Nano Lett.* **2008**, *8*, 689−692.
(5) Azulai, D.; Belenkova, T.; Gilon, H.; Barkay, Z.; Markovich, G. *Nano Lett.* **2009**, *9*, 4246−4249.
(6) Hu, L.; Kim, H. S.; Lee, J.-Y.; Peumans, P.; Cui, Y. *ACS Nano* **2010**, *4*, 2955−2963.
(7) Wu, Z. C.; Chen, Z. H.; Du, X.; Logan, J. M.; Sippel, J.; Nikolou, M.; Kamaras, K.; Reynolds, J. R.; Tanner, D. B.; Hebard, A. F.; Rinzler, A. G. *Science* **2004**, *305*, 1273−1276.
(8) Hu, L.; Hecht, D. S.; Gruner, G. *Nano Lett.* **2004**, *4*, 2513−2517.
(9) Dan, B.; Irvin, G. C.; Pasquali, M. *ACS Nano* **2009**, *3*, 835−843.
(10) Becerril, H. A.; Mao, J.; Liu, Z.; Stoltenberg, R. M.; Bao, Z.; Chen, Y. *ACS Nano* **2008**, *2*, 463−470.
(11) Eda, G.; Lin, Y. Y.; Miller, S.; Chen, C. W.; Su, W. F.; Chhowalla, M. *Appl. Phys. Lett.* **2008**, *92*, 233305.
(12) Wang, X.; Zhi, L. J.; Mullen, K. *Nano Lett.* **2008**, *8*, 323−327.
(13) Wan, Q.; Dattoli, E. N.; Fung, W. Y.; Guo, W.; Chen, Y.; Pan, X.; Lu, W. *Nano Lett.* **2006**, *6*, 2909−2915.
(14) O'Dwyer, C.; Szachowicz, M.; Visimberga, G.; Lavayen, V.; Newcomb, S. B.; Sotomayor Torres, C. M. *Nat. Nanotechnol.* **2009**, *4*, 239−244.
(15) Yu, H. K.; Dong, W. J.; Jung, G. H.; Lee, J.-L. *ACS Nano* **2011**, *5*, 8026−8032.
(16) Ederth, J.; Johnsson, P.; Niklasson, G. A.; Hoel, A.; Hultåker, A.; Heszler, P.; Granqvist, C. G.; van Doorn, A. R.; Jongerius, M. J.; Burgrad, D. *Phys. Rev. B* **2003**, *68*, 155410.
(17) Gilstrap, R. A., Jr.; Capozzi, C. J.; Carson, C. G.; Gerhardt, R. A.; Summers, C. J. *Adv. Mater.* **2008**, *20*, 4163−4166.
(18) Bühler, G.; Thölmann, D.; Feldmann, C. *Adv. Mater.* **2007**, *19*, 2224−2227.
(19) Arsenault, E.; Soheilnia, N.; Ozin, G. A. *ACS Nano* **2011**, *5*, 2984−2988.
(20) Dattoli, E. N.; Lu, W. *MRS Bull.* **2011**, *36*, 782−788.
(21) Jeong, J.-A.; Kim, H.-K. *Curr. Appl. Phys.* **2010**, *10*, e105−e108.
(22) Lee, J.; Lee., S.; Li, G.; Petruska, M. A.; Paine, D. C.; Sun, S. *J. Am. Chem. Soc.* **2012**, *134*, 13410−13414.
(23) Puetz, J.; Al-Dahoudi, N.; Aegerter, M. A. *Adv. Eng. Mater.* **2004**, *6*, 733−737.
(24) Puetz, J.; Aegerter, M. A. *Thin Solid Films* **2008**, *516*, 4495−4501.
(25) Heusing, S.; de Oliveira, P. W.; Kraker, E.; Haase, A.; Palfinger, C.; Veith, M. *Thin Solid Films* **2009**, *518*, 1164−1169.
(26) Maksimenko, I.; Wellmann, P. *Thin Solid Films* **2011**, *519*, 5744−5747.
(27) Maksimenko, I.; Kilian, D.; Mehringer, C.; Voigt, M.; Peukert, W.; Wellmann, P. J. *J. Appl. Phys.* **2011**, *110*, 104301.
(28) Bichler, C. H.; Langowski, H. −C.; Moosheimer, U.; Seifert, B. *J. Adhes. Sci. Technol.* **1997**, *11*, 233−246.
(29) Weidner, S.; Kühn, G.; Decker, R.; Roessner, D.; Friedrich, J. *J. Polym. Sci., Polym. Chem.* **1998**, *36*, 1639−1648.
(30) Le, Q. T.; Pireaux, J. J.; Caudano, R.; Leclere, P.; Lazzaroni, R. *J. Adhes. Sci. Technol.* **1998**, *12*, 999−1023.
(31) Greenwood, O. D.; Hopkins, J.; Badyal, J. P. S. *Macromolecules* **1997**, *30*, 1091−1098.
(32) Boyd, R. D.; Badyal, J. P. S. *Macromolecules* **1997**, *30*, 3658−3663.
(33) Yun, J.; Lee, S.; Bae, T. S.; Yun, Y.; Lee, S.; Kwon, J. D.; Lee, G. H. *Plasma Process. Polym.* **2011**, *8*, 815−831.
(34) Haacke, G. *J. Appl. Phys.* **1976**, *47*, 4086−4089.
(35) Cairns, D. R.; Witte, R. P.; Sparacin, D. K.; Sachsman, S. M.; Paine, D. C.; Crawford, G. P.; Newton, R. R. *Appl. Phys. Lett.* **2000**, *76*, 1425−1427.
(36) Park, S. K.; Han, J. I.; Moon, D. G.; Kim, W. K. *Jpn. J. Appl. Phys.* **2003**, *42*, 623−629.
(37) Leterrier, Y.; Médico, L.; Demarco, F.; Månson, J. A. E.; Betz, U.; Escolà, M. F.; Olsson, M. K.; Atamny, F. *Thin Solid Films* **2004**, *460*, 156−166.
(38) Stoney, G. G. *Proc. R. Soc. London, Ser. A* **1909**, *82*, 172−175.